11-2014

Study of As(III) and As(V) Oxoanion Adsorption onto Single and Mixed Ferrite and Hausmannite Nanomaterials

Sandra Garcia

Saima Sardar

Stephanie Maldonado

Velia Garcia

C Tamez

See next page for additional authors

Recommended Citation

Garcia S, Sardar S, Maldonado S, Garcia V, Tamez C, Parsons JG. Study of As(III) and As(V) Oxoanion Adsorption onto Single and Mixed Ferrite and Hausmannite Nanomaterials. Microchem J. 2014;117:52-60. doi:10.1016/j.microc.2014.06.008

Published in final edited form as:
Microchem J. 2014 November 1; 117: 52–60. doi:10.1016/j.microc.2014.06.008.

Study of As(III) and As(V) Oxoanion Adsorption onto Single and Mixed Ferrite and Hausmannite Nanomaterials

Sandra Garcia, **Saima Sardar**, **Stephanie Maldonado**, **Velia Garcia**, **C. Tamez**, and **J. G. Parsons***
Department of Chemistry the University of Texas-Pan American 1201 W University Dr. Edinburg TX, 78539

Abstract

The removal of arsenic(III) and arsenic(V) from an aqueous solution through adsorption on to Fe_3O_4, $MnFe_2O_4$, 50% Mn substituted Fe_3O_4, 75% Mn substituted Fe_3O_4, and Mn_3O_4 nanomaterials was investigated. Characterization of the nanomaterials using XRD showed only pure phases for Mn_3O_4, $MnFe_2O_4$, and Fe_3O_4. The 50% and 75% substituted nanomaterials were found to be mixtures of Mn_3O_4 and Fe_3O_4. From batch studies the optimum binding pH of arsenic(III) and arsenic(V) to the nanomaterials was determined to be pH 3. The binding capacity for As(III) and As(VI) to the various nanomaterials was determined using Isotherm studies. The binding capacity of Fe_3O_4 was determined to be 17.1 mg/g for arsenic(III) and 7.0 mg/g for arsenic(V). The substitution of 25% Mn into the Fe_3O_4 lattice showed a slight increase in the binding capacity for As(III) and As(VI) to 23.8 mg/g and 7.9 mg/g, respectively. The 50% substituted showed the maximum binding capacity of 41.5 mg/g and 13.9 mg/g for arsenic(III) and arsenic(V). The 75% Mn substituted Fe_3O_4 capacities were 16.7 mg/g for arsenic(III) and 8.2 mg/g for arsenic(V). The binding capacity of the Mn_3O_4 was determined to be 13.5 mg/g for arsenic(III) and 7.5 mg/g for arsenic(V). In addition, interference studies on the effects of SO^{2-}_4, PO^{3-}_4, Cl^-, and NO^-_3 investigated. All the interferences had very minimal effects on the As(III) and As(V) binding never fell below 20% even in the presence of 1000 ppm interfering ions.

1. Introduction

Arsenic is an element that is ubiquitous throughout the world: found in the earth's crust, in both surface and ground water, and within in the human body [1,2]. The toxic effects of arsenic in humans come from the ingestion of arsenic contaminated food and water. However, in general the inorganic compounds of arsenic more toxic than the organic arsenicals and are common contaminates in drinking water [1]. The As(III) (arsenite) compounds are much more toxic than the As(V) (arsenate) compounds [2]. Arsenic has been

*Corresponding author to whom all correspondence should be addressed. Ph: (956)665-7462, Fax: (956)665-5006, parsonsjg@utpa.edu..

linked to variety of health effects when ingested in small consistent dosages through combined food or drinking water [1,2]. The effects of As include abnormal skin conditions, gastrointestinal problems, neurological effects, and diabetes [1-5]. Furthermore, links between arsenic exposure and several types of cancer have been established, which including: lung, skin, kidney, liver, and prostate [4]. Due to the numerous health risks the Environmental Protection Agency has set the MCL of arsenic in drinking water from to 0.010 parts per million in an effort to reduce number the health effects caused by the long-term ingestion of arsenic in the US population. [2, 6]

There are several methods to remove arsenic from drinking water, which include precipitation, ion exchange, membrane process, coagulation, and adsorption [7-12]. In general technologies to remove arsenic from drinking water are generally non-specific and expensive to water treatment plants. However, nano-adsorbents may provide a more cost effective technology for the removal of As(III) and As(V) from contaminated water [10, 11, 14-17]. Nanomaterials are a promising emerging technology with many different applications due to their enhanced reactivity and high surface area to volume ratio. Adsorbents have been studied for the remediation/removal of many different ions from aqueous solution. More recently, nanomaterials have been investigated for the removal of inorganic contaminates from aqueous solution, including the inorganic forms of arsenic. Adsorbents such as activated alumina, clay based materials, red mud (the waste from aluminum processing), Al-WTR (water treatment residuals) Fe-WTR, iron oxide materials, manganese oxide nanomaterials, granular ferric oxide, as well as metal sulfide nanomaterials [14-19].

Studies investigating the adsorption of As(III) and As(V) using activated alumina have shown the effect of pH, surface oxidation, and competing ions [6]. It has been shown that between pH 7and 8 activated alumina has a net positive charge, which showed a preference for the adsorption of anions from solution including arsenic. Acidic pHs are generally considered optimum for arsenic removal with activated alumina. Genc-Fuhrman et al. found arsenic adsorption using activated red mud was effective for As(V) adsorption. The optimum pH for As(V) adsorption was 4.5 with a removal of approximately 100%. In addition, the desorption of As(V) was found to be optimum pH 11.6 with a maximum desorption of 40%. In contrast, the optimum pH for As(III) binding was found to be 8.5, and the removal efficiency was dependent on the initial As(III) concentration [20]. In a similar study Altundogan et al. also investigated the application of activated red mud on arsenic removal [21]. Altundogan et al. showed the optimum binding pH range for As(III) was from 5.8 to .5 and the optimum pH range for As(V) binding was from 1.8 to 3.5; with a maximum removal of As(V) was 96.52% and 87.54% for As(III) [21].

Adsorption techniques using nanoparticles have shown promise as being an effective technique to remove ions from water. Luther et al. showed the adsorption of As(III) to Fe_2O_3 and Fe_3O_4 nanomaterials were 1.250 mg/g and 8.196 mg/g after one hour of contact time, respectively [22]. However, at a contact time of 24 hours the 20 mg/g for Fe_2O_3 and 5.680 mg/g for Fe_3O_4, was observed for As(III) binding to the nanomaterials [22]. The binding capacities for As(V) were lower in magnitude at both the one hour and 24 hour contact time. The Fe_2O_3 nanomaterials had similar capacities of 4.6 mg/g and 4.9 mg/g for

the one hour and 24 hour contact times for As(V) binding, respectively. Whereas, the Fe_3O_4 nanomaterial had capacities of 6.7 and 4.8 for the 1 and 24 hour contact times, respectively for As(V) binding [22]. Parsons et al. have investigated the binding of As(III) and As(V) binding to Mn_3O_4, a $MnFe_2O_4$ and Fe_3O_4 nanomaterials [11]. In this study the maximum binding capacity for the Fe_3O_4 was 0.0322 mg/g and 1.575 mg/g for the As(III) and As(V), respectively [11]. The binding capacity of the $MnFe_2O_4$ nanomaterial had a binding capacity of 0.718 and 2.212 mg/g for As(III) and As(V) respectively. The Mn_3O_4 nanomaterial had a binding capacity of 0.0089 and 0.211 for the As(III) and As(V), respectively [11]. In addition, at the concentrations used the pH dependency of the arsenic binding was pH dependent increasing from pH 2 to pH 6. Al-WTRs have been shown to have varying between capacities for As(III) and As(V) of 1,8-15 mg/g for As(V) and between 7.500-15 mg/g for As(III) after 48 hours of equilibrium with a pH range from 6-6.5 [17]. Latterite iron concretions have been shown to have As sorption capacities of 909 ug/g and 714 ug/g for As(III) and (V), respectively at pH 7 [23].

In the present study the effect of Manganese (Mn) substitution into the Fe_3O_4 lattice from 25% to 75% and pure Mn_3O_4 on arsenic(III) and arsenic(V) adsorption. The nanomaterials were synthesized through a precipitation process and characterized using XRD. Batch studies were performed to determine the effect of pH and the effect of interfering ions on the adsorption of both As(III) and As(V) onto the different metal oxide nanomaterials. In addition, the binding capacities for the different materials were determined using isotherm studies, which were found to follow the Langmuir Isotherm.

2. Methodology

2.1 Synthesis of the nanoadsorbents

The synthesis of the Fe_3O_4 nanomaterial a 1.0 L of metal ion solution containing 30.0 mM of Fe(II) (from $FeCl_2$), was prepared. For the Manganese substituted nanomaterials a specific percentage of the Iron(II) was substituted with manganese(II) (from $MnCl_2$). The solution for the 25% Mn −75%Fe consisted of 7.5 mM Mn^{2+} and 22.5 mM Fe^{2+}. The solution for the synthesis of the 50% Mn-50% Fe, contained 15 mM Mn^{2+} and 15 mM Fe^{2+}. The 75% Mn-25%Fe was synthesized from a solution containing 22.5 mM Mn^{2+} and 7.5 mM Fe^{2+}. Finally the solution for the synthesis of the Mn_3O_4 nanomaterial consisted of a 30.0 mM solution of Mn^{2+}. The prepared solutions were then titrated using 100 mL of a 1.0 M NaOH solution to obtain a 1:3 ratio of M^+:OH^-, over approximately 2 hours. The samples were then heated 90°C for hour under constant stirring. Subsequent to heating the samples were then cooled to room temperature and centrifuged at 3000 rpm (Fisher Scientific 8K, Houston, TX) for 5 min. The supernatants were discarded and the solid sample was suspended in 18 Mω deionized (DI) water and centrifuged again to remove any unreacted starting material and reaction byproducts of the reaction. The samples were washed twice with 18 MΩ DI to ensure clean materials for the subsequent reactions. After washing, the nanomaterials were oven dried at 70 °C until dry.

2.2 XRD characterization

The samples were characterized using X-ray diffraction in combination and fitted for phase using the FullProf Suite programs. The XRD patterns were collected at room temperature using a Rigaku Miniflex X-ray powder diffractometer (Rigaku Coporation, The Woodlands, TX). The samples were homogenized using a mortar and pestle and then placed on an aluminum sample holder. The samples were then diffracted from 20 to 60 degrees in 2θ using a 2 s counting time and a stepping rate of 0.001 °/min. The fittings were performed using crystallographic data from the literature and the FullProf 2001 Suite programs using the Le Bail fitting procedure with fixed intensities of the diffraction lines [24-27]. The average grain size of the nanoparticles was determined using the Scherrer's equation and a Gaussian fitting of three independent diffraction peaks.

2.3 pH profile

The effect of pH binding of arsenic(III) and arsenic(V) was evaluated from pH 2 to 6 on the synthesized nanoadsorbents Fe_3O_4, 25 %Mn substituted Fe_3O_4, 50 %Mn substituted Fe_3O_4, 75 %Mn substituted $MnFe_3O_4$, and the Mn_3O_4. Arsenic (III) and Arsenic (V) solutions were prepared at a concentration of 300 ppb in 18 MΩ DI water and pH adjusted to pH 2.0, 3.0, 4.0, 5.0 and 6.0. The pH of the solution was adjusted using either dilute sodium hydroxide or dilute nitric acid. A 4.0 mL aliquot of the pH adjusted solutions added to 10 mg of the nanomaterial in a 5 mL polyethylene test tube. The reaction mixture was capped, placed on a rocker, and equilibrated for 1 hour. Control samples containing only the arsenic ions were treated the same as the samples. Both samples and control solutions performed in triplicate for statistical purposes. After equilibration, the samples were centrifuged at 3000 RPM for 5 min. The supernatant from each tube was saved for analysis using ICP-OES. All ICP-OES analyses were performed on a Perkin Elmer Optima 8300 DV (Perkin-Elmer, Shelton, CT). All calibration curves had correlation coefficients (R^2) of 0.99 or better.

2.4 Capacity studies

A mass of 10 mg of each of the nanomaterial were weighted out in triplicate, and placed in individual test tubes. The 10 mg of nanomaterial then had 4 mL of a either an As(III) or As(V) solution with concentrations of either 3ppm, 30ppm, 150ppm, 300ppm or 1,000ppm, which was previously adjusted to pH 3, was added to the tube. The nanomaterials and arsenic solutions were capped, placed on a rocker, and equilibrated for one hour. In addition, control samples containing only the As(III) or As(V) ions were also equilibrated for one hour. Subsequent to equilibration, the sample and control solutions were centrifuged at 3000 RMP for 5 minutes. The supernatants were decanted and saved for analysis using ICP-OES. All ICP-OES calibration curves used had a minimum R^2 of 0.99.

2.5 Interference studies

A mass of 10 mg of the nanomaterials was weighed in triplicate and placed into a 5 mL test tube. A 4 mL aliquot of a solution containing either 300 ppb As(III) or As(V) with varying concentrations of the ions Cl^-, NO^-_3, SO^{2-}_4, or PO^{3-}_4, pH adjusted to 3. The interfering solutions contained individual ion concentrations of 0.3, 3, 30, 300, or 1000ppm. In addition, combined interference samples were prepared containing all the interfering ions

together at 0.3, 3, 30, 300, or 1000ppm, in the presence of 300 ppb As(III) or As(V). In addition, control samples containing only the arsenic and the interfering ions were prepared and treated the same as the samples. All samples and control reactions were performed in triplicate for statistical purposes. The samples and controls were placed on a rocker and equilibrated for one hour. Subsequent to equilibration, the reaction and control samples were centrifuged at 3000rpm for 5 minutes and the supernatants were saved for analysis using ICP-OES. All ICP-OES calibration curves obtained had a minimum R^2 0.99.

2.6 ICP-OES analysis

ICP-OES analysis was performed using a Perkin Elmer Optima 8300 DV (Perkin Elmer, Shelton CT) ICP-OES. The calibrations curves for the low concentration reactions were performed from 0.01 ppm to 0.5 ppm using. The higher concentration, the capacity studies, samples had calibration curves extended to 50 ppm. Samples that were above 50 ppm in concentration were diluted to run within the calibration range. All calibration curves obtained for analysis had R^2 of 0.99 or better. The operational parameters for the ICP-OES are shown below in Table 1.

3.0 Results and Discussion

3.1 XRD Results

Figure 1 shows the diffraction patterns obtained for the synthesized nanomaterials after drying. In addition, the refined lattice parameters for the substitution of the Mn into the Fe_3O_4 lattices from the fitting are shown in Table 2. The diffraction patterns were fitted for both phase of the material using the Le Bail fitting procedure in the Fullproff software [24]. As can be seen in the fitting shown in Figure 1 A the Fe_3O_4 sample diffraction patterns matches very well with the diffraction pattern for Magnetite. This is indicated by the presence of the diffraction peaks (Bragg Peaks) at 30.19° (220), 35.56° (311), 37.20° (222), 43.22° (400), 53.63° (422) and the diffraction peak located at 57.17° (333/511), which has been shown in the literature corresponding to a space group of FD-3M [25]. The 25% Mn-75Fe material presented in Figure 1 B shows the same peaks indicating that the material retains the Fe_3O_4 structure and lattice, which is the MnFe2O4 crystal lattice [26]. However, the 50% Mn-50% Fe material presented in Figure 1 C shows the presence of Mn_3O_4 in the sample. The presence of the Mn_3O_4 is indicated by the appearance of the shoulder on the Fe_3O_4 311 (35.56°) diffraction plane, which corresponds to the 211 (36.14°) and 202 (36.45°) diffraction planes of Mn_3O_4 phase [27]. It should be noted here the diffraction patterns with two sets Bragg peaks that the higher Bragg peaks are for the Fe_3O_4 phase and the lower Bragg peaks are for the Mn_3O_4 phase. Furthermore, the 75% Mn-25% Fe shown in Figure 1 D shows the development of much stronger diffraction planes of the Mn_3O_4 phase. From the 75% Mn-25% Fe reaction product diffraction peaks in the sample corresponding to the 220 (30.19°), 311 (35.56°), 222 (37.20°), 400 (43.22°), and the 333/511 (57.17°) diffraction planes for Fe_3O_4 are visible. In addition, in the 75% Mn-25% Fe material the 112 (28.88°), 103 (32.33°), 211 (36.14°), 202 (36.45°), 004 (38.13°), and the 213 (45.38°) are visible in the sample [27]. Figure 1 D presents the diffraction pattern of the Mn_3O_4 nanomaterial as synthesized as can from the fitting of this diffraction pattern the following diffraction peaks were found 28.88° (112), 30.96° (200), 32.33° (103), 36.14°

(211), 36.45° (202), 38.13° (004), 44.36° (220), 45.38° (213), 49.83° (204), 50.76° (105), 53.80° (312), 55.96° (303), 58.43° (321), 59.83° (224), which correspond to Mn_3O_4 in the I41/AMD lattice [27]. In addition, the average grain size of the nanomaterials was determined using the Scherer equation, which are presented in Table 3. As can be seen in Table 3 the average grain sizes of the nanomaterials do not change dramatically between the different preparation of the materials. All the synthesized nanomaterials had average grain sizes ranging from 15-20 nm. Only in the 50% Mn-50% Fe mixed phase material that the average grain size of the Mn_3O_4 nanomaterials could not be determined.

3.2 pH studies

The binding of both As(III) and As(V) to the synthesized nanomaterials are varying pH from 2.0 to 6.0 is shown in Figures 2A through E. As can be seen from Figure 2 the binding of As(III) to the Fe_3O_4 and substituted $MnFe_2O_4$ is for the most part pH independent from pH 2 through pH 6. However, the binding of the As(III) to the Mn_3O_4 nanomaterial becomes pH dependent with decreasing binding with increasing pH. As can be seen in Figure 3 E the binding is almost eliminated at pH 5. In addition the As(VI) anion also follows a similar tend as the As(III) oxoanion. However, the binding of As(V) to the MnFe2O4 nanomaterial appears to be affected by pH, showing a decrease in the binding efficiency from approximately 100% at pH 3 to approximately 60% at pH 5. The high binding of both As(III) and As(V) to iron oxide based nanomaterials has been shown in the literature to be pH independent for both As(III) and As(V) to Fe_3O_4 [23]. The decrease in the binding observed with the As(III) and As(V) binding to the $MnFe_2O_4$ nanomaterial and the Mn_3O_4 nanomaterial may be due to the presence of the Mn ions in the phase. The XRD data suggests that the Mn in the $MnFe_2O_4$ material is substituted into the material, whereas in the higher combination materials there are two distinct phases the Fe_3O_4 and Mn_3O_4. The independence in the binding of the As(III) and As(V) for the 50% Mn sample and the 75% Mn sample may be due to the presence of the Fe_3O_4 phase, which is performing the binding and not the Mn_3O_4 phase above pH 3. Whereas, the 25% phase the substitution of the Mn into the Fe sites is suggested by the diffraction data and the reduction of the lattice parameters as shown in Table 2. The substitution of the Mn^{2+} in crystal for the Fe^{2+} may actually inhibit the binding efficiency of the material. Mn based materials have shown to produce redox coupling with chromium and arsenic ions in solution at low pH [28, 29]. The binding may be inhibited or decrease above pH 4 in the Mn_3O_4 due to the inability of the material to produce a redox couple with the ions. Alternatively the PZC (point of zero charge) of the nanomaterials plays an important role for the binding of metal ions to nanomaterials. From the literature it can be seen that many of metal oxide nanomaterials especially Fe_3O_4 have PZC above pH 6 (ranges from 6.5 to 9.9) [30]. However, Mn_3O_4 has a PZC around pH 4.5, which helps to explain the dramatic decrease in binding observed between pH 4 and pH 5 for the Mn_3O_4 nanomaterial as seen Figure 2 E [31]. At a pH of 4.5 the nanomaterial becomes neutral change and there is no preference in the binding. However, at pH 5 the nanomaterial becomes negatively charged at the surface and will repel the As(III) and As(V) oxoanions from binding to the surface. This effect is not observed in the 50% and the 75% because of the presence of both Fe_3O_4 and Mn_3O_4 phases however the Fe_3O_4 phase would be responsible for the binding of the As(III) and As(V) from solution.

3.3 Isotherm studies

Table 4 shows the parameters derived from the isotherm studies which were found to follow the Langmuir isotherm. As can be seen in Table 4 the correlation coefficient for the isotherm studies of As(III) and As(V) binding to the nanomaterials are 0.99 to 1.0, indicating a strong correlation to the Langmuir isotherm. The linearized form of the Langmuir equation is shown below:

$$\frac{1}{q_e} = \left(\frac{1}{Q_0 b} * \frac{1}{C_e}\right) + \frac{1}{Q_o}$$

Where C_e is the equilibrium concentration, Q_0 is the capacity of the nanomaterial, q_e is the amount of arsenic bound/mg of material, b is a parameter related to the material and to the solution parameters such as pH and ionic strength.

The isotherm study indicates that the binding of arsenic from aqueous solution is occurring on the surface in a monolayer of arsenic ions. Table 5 shows the results of the calculated binding capacities of the different synthesized nanomaterials. As can be seen in Table 5 the As(III) binding capacities are at least twice those determined for the As(VI) ions. The binding capacity of the nanomaterials was found to increase from pure Fe_3O_4 and maximize at the 50% Mn-50% Fe material. Both the As(III) and As(V) ion binding capacities almost double at the 50 % Mn-50% Fe material compared to the Fe_3O_4 nanomaterials. In addition, the enhancement in the binding capacity diminishes again at the 75% Mn-25%Fe sample and continues to get smaller with the Mn_3O_4 nanomaterial. The enhancement observed in the binding when Mn is added to the Iron material, initially may be do the substitution of the Mn in the Fe_3O_4 lattice. However, at higher Mn percentage a second phase (Mn_3O_4) develops as can be seen in Figure 1 C, a shoulder develops on the Fe 311 plane which corresponds to the Mn_3O_4 211 plane. Extremely small Mn_3O_4 nanomaterials are suggested by the presence of the diffraction planes for the Mn_3O_4 material. The small particles present in the 50% Mn-50% Fe may be responsible for the enhanced binding observed in the material. The synthesized Mn-Fe nanomaterials do have capacities similar and in many cases much greater than those shown in the literature for similar types of materials. For example Al-wtr (Al based water treatment residuals) have shown capacities of 7.5-15.0 mg/g after two days of equilibration [19]. In another study using 25% doping of diatomite the capacity was determined to be 10.8 mg/g after 8 hours of contact time [32]. In addition the binding of As(V) has been shown to have capacities that range from 0.6-8.6 mg/g which is material dependent. Hematite particles have shown capacities ranging from 0.16 to 0.20 mg/g. However, Goethite, a FeOOH material has shown a sorption capacity of 11.2 mg/g for arsenic (V) and 12.2 mg/g for As(III) [33]. Iron oxides show dramatic differences in their binding capacities for arsenic ions. The differences observed in the binding capacities of metal oxides can be correlated to the ions present in the materials, as well as the particle size, and the crystallinity of the particles used in the studies. Similarly, Mn based materials have been shown to be effective in the removal of As(III) and As(V) from aqueous solution. MnO_2 loaded polystyrene resin has shown to have a capacity of 53 mg/g for As(III) and 22 mg/g for As(V) [35]. Whereas, manganese based ore has been shown to have a capacity of 0.53 mg/g for As(III) and 15.38 mg/g for arsenic(V) at pHs around 6.5 [36]. In addition, a

mixture of FeMn minerals has shown capacities of 14.7 and 8.5 mg/g for As(III) and As(V) at pH 3 [37]. However, in the present study the results of the isotherm studies show exceptional binding capacities especially with the 25%Mn-75%Fe and the 50%Mn-50% Fe synthesized materials with capacities of 23.8 mg/g and 41.5 mg/g for the arsenic(III) ion and 7.9 and 13.9 mg/g for the arsenic(VI) ions. The observed high binding capacities may be due to redox coupling within the materials which has been suggested in the literature for the removal or arsenic with different metal oxides including Fe and Mn based materials. The removal of As(III) has through redox processes has been shown in materials containing Fe and Mn(IV and VII) to form As(VI) which is then adsorbed to the material [37].

3.4 Interference study

The results for the interference studies on the binding of As(III) and As(V) to the different nanomaterials are shown in Figure 3 and 4, respectively. As can be seen in Figure 3 the As(III) binding the effects of the different anions on As(III) sorption to the nanomaterials are varying. As can be seen in Figure 3 Cl^{-}, PO^{3-}, the $SO^{2-}{}_4$, have little to no effect on the binding of As(III) to the nanomaterials. $SO^{2-}{}_4$ does have an initial effect on the binding at low concentrations however, once the concentration of the anion reaches 30 ppm the effects is no longer shown in the binding solution. However, nitrate has an effect on the binding of the As(III) to the 25%Mn-75%Fe. The binding of the As(III) remains below 60% (Figure 3 B) in the presence of nitrate to the 25%Mn-75%Fe nanomaterial. In addition, the reduced binding of the As(III) to the 25%Mn-75%Fe nanomaterial is observed in the solutions with combinations of all the interfering ions as can be observed in Figure 3 E. However, in the combined interference solutions with concentrations of interfering present above 30 ppm the binding was observed continually decrease to 1000 ppm concentration of all ions in solution. However, with respect to molar ratios this is a 16,301 moles of interfering ions to every 1 mole of As in solution. Many of the studies in the literature for the binding of As(III) and As(V) show that either $PO^{3-}{}_4$ or $SO^{2-}{}_4$ have a negative effect on the binding of arsenic from solution [38-40]. However, in the present study there is no apparent effect on the binding by these anions which is adsorbent material dependent. The non-observed reduction in binding in arsenic the presence of either $PO^{3-}{}_4$or $SO^{2-}{}_4$ may be a surface effect of the synthesized nanomaterials, the number of active sites for adsorption of the Arsenic. Alternatively, the materials synthesized under the conditions used in this study may present a material that has preferential binding of Arsenic over other anions.

Similar results were obtained with the As(V) binding to the different nanomaterials in the presence of Cl^{-}, NO^{-3}, $SO^{2-}{}_4$, $PO^{3-}{}_4$,and in the presence of all the interfering ions combined in solution as compared to the As(III) binding studies. As can be observed in Figure 4 A the Cl^{-} anion had no effect on the binding of the As(V) to any of the studied nanomaterials. Whereas the $PO^{3-}{}_4$ anion had a detrimental effect on the binding of the of the As(V) ion to the most of the nanomaterials with the exception of the Mn_3O_4 nanomaterial. The interference on the binding was observed at concentrations of 30 ppm and above. The $PO^{3-}{}_4$ anion had the least effect on both the pure Fe_3O_4 and 75%Mn-25%Fe as can be seen in Figure 4B. Whereas, the mixed phases were effected the most by the $PO^{3-}{}_4$ phase. There appears to be some synergistic effect at the high percentage of Mn with the Fe_3O_4 phase. As was observed from the diffraction data the 25% Mn-75% Fe is a pure material. However, as

the percentage of Mn is increase there appears to be the generation of two different phases in the material until a pure Mn_3O_4 phase is synthesized. The presence of the two phases at approximately the same concentration/same size seems to have a synergistic effect on the binding in the presence of the nitrate anion. The literature suggests that PO^{3-}_4 can compete with arsenic adsorption due to the formation of surface complexes [38-40]. The effect of phosphate on the binding of the nanomaterials studied here only show detrimental effects at concentration of 300 ppm and above. It is interesting that the pure phase Mn_3O_4 nanomaterial exhibits the largest binding decreases in the presence of the PO^{3-}_4 anion followed by the 25% Mn-75%Fe and the 50% Mn-50%Fe. On the other hand the pure phase Fe_3O_4 nanomaterial and the 75% Mn-2%Fe materials are the least effected by the PO^{3-}_4 concentrations. Figure 4 C shows the binding of the As(V) in the presence of NO^{-}_3 anion. As can be seen in Figure 4C the binding of the As(V) ions in the presence of nitrate starts to be suppressed at NO^{-}_3 concentrations of above 3 ppm. The NO^{-}_3 effect on binding is carried through to 1000 ppm. The effect of NO^{-}_3 on the binding increases with increasing concentration for all the materials studied. However, the binding of the As(V) to the pure Fe_3O_4 nanomaterial appears to be affect the most by the NO^{-}_3 in solution. Also the As(V) binding to the pure Mn_3O_4 nanomaterials is also effected greater than the As(V) binding to the substituted materials and the mixed phase materials. Figure 4 D shows the effect of SO^{2-}_4 concentration on the binding of As(V) from solution. As can be seen in Figure 4D the sulfate anion has little to no effect on the binding at concentrations up to and including 300 ppm. However at concentrations greater than 300 ppm the binding is decreased at 1000 ppm the binding of the As(V) anion ranges from 20-50% for all the materials studied. This decrease in Binding observed at 1000 ppm SO^{2-}_4 is actually small considering that the molar ratio of 1 As: 2600 SO^{2-}_4 anions is present in the binding solution. The data indicates that all the materials have some selectivity towards binding As(V) over the SO^{2-}_4 anions from aqueous solution. Figure 4 E shows the binding of the As(V) anions in the presence of all the interfering ions combined in solution. As can be seen in the Figure 4 E the binding is not affected as greatly, as in the study of the individual anions in solution. The reduced interference in solution observed in the combined interference study may be a synergistic effect of the combination of the anions. The interaction of all the ions in solution may be interacting with each other and the arsenic causing the binding of the As to the nanomaterial to be higher than what is observed with the ion alone. In addition, the combined interference never completely eliminates the binding of the arsenic(V) to the different nanomaterials. At a concentration of 1000 ppm of all the interferences combined in solution the lowest observed binding is to the 25% Mn −75% Fe material which was approximately 20%. However, this is a molar ratio of 1 As: 16308 interfering ions which shows selectivity of the nanomaterials to the binding of the As(V) anion. The literature suggests that PO^{3-}_4 can compete with arsenic adsorption due to the formation of surface complexes [39]. It has been shown that found that common anions such as sulfate, chloride, or bicarbonate in general only slightly interfere with the sorption of As(III) and As(V) from aqueous solution to iron based nanomaterials [22]. The binding of As(V) to the mixed phase nanomaterials (above 50% Mn Substitution) and the pure Mn_3O_4 in the presence of PO^{3-}_4 were affected the binding the greatest.

Acknowledgments

Authors would like to thank the NIH UTPA RISE program (Grant Number 1R25GM100866-01) and the HHMI (grant number 52007568). The Authors acknowledge financial support from the Welch Foundation for supporting the Department of Chemistry (Grant number GB-0017) and UTPA for sponsoring this research project.

References

1. Feng L, Cao M, Ma X, Zhu Y, Hu C. Superparamagnetic high-surface-area Fe_3O_4 nanoparticles as adsorbents for arsenic removal. J. Hazard. Mater. 2012; 217-218:439–444. [PubMed: 22494901]
2. Kundu S, Gupta AK. Arsenic Adsorption onto Iron Oxide-coated Cement (IOCC): Regression Analysis of Equilibrium Data with Several Isotherm Models and Their Optimization. Chem. Eng. J. 2006; 122:93–106.
3. Lievremont D, Bertin PN, Left M-C. Arsenic in contaminated waters: Biogeochemical cycle, microbial metabolism and biotreatment processes. Biochimie. 2009; 91:1229–1237. [PubMed: 19567262]
4. Ng JC, Wang J, Shraim A. A global health problem caused by arsenic from natural sources. Chemosphere. 2003; 52:1353–1359. [PubMed: 12867164]
5. Rahman M, Tondel M, Ahmad SA, Axelson O. Diabetes Mellitus Associated with Arsenic Exposure in Bangladesh. Am. J. Epidemiol. 1998; 148:198–203. [PubMed: 9676702]
6. Giles DE, Mohapatra M, Issa TB, Anand S, Singh P. Iron and aluminium based adsorption strategies for removing arsenic from Water. J. Environ. Manage. 2011; 92:3011–3022. [PubMed: 21871703]
7. Song S, Lopez-Valdivieso A, Hernandez-Campos DJ, Peng C, Monroy-Fernandez MG, Razo-Soto I. Arsenic removal from high-arsenic water by enhanced coagulation with ferric ions and coarse calcite. Water Res. 2006; 40:364–372. [PubMed: 16352327]
8. Matsunaga H, Yokoyama T, Eldridge RJ, Bolto BA. Adsorption characteristics of arsenic(II1) and arsenic(V) on iron(III)-loaded chelating resin having lysine-N^{α},N^{α}-diacetic acid moiety. React. Funct. Polym. 1996; 29:167–174.
9. Zhao Z, Jia Y, Xu L, Zhao S. Adsorption and heterogeneous oxidation of As(III) on ferrihydrite. Water Res. 2011; 45:6496–6504. [PubMed: 22000059]
10. Gonzalez CM, Hernandez J, Parsons JG, Gardea-Torresdey JL. A study of the removal of selenite and selenate from aqueous solutions using a magnetic iron/manganese oxide nanomaterial and ICP-MS. Microchem. J. 2010; 96:324–329.
11. Parsons JG, Lopez ML, Peralta-Videa JR, Gardea-Torresdey JL. Determination of arsenic(III) and arsenic(V) binding to microwave assisted hydrothermal synthetically prepared Fe_3O_4, Mn_3O_4, and $MnFe_2O_4$ nanoadsorbents. Microchem. J. 2009; 91:100–106.
12. Mohana D, Pittman CU Jr. Arsenic removal from water/wastewater using adsorbents A critical review. J. Hazard. Mater. 2007; 142:1–53. [PubMed: 17324507]
13. Feng L, Cao M, Ma X, Zhu Y, Hu C. Superparamagnetic high-surface-area Fe_3O_4 nanoparticles as adsorbents for arsenic removal. J. Hazard. Mater. 2012; 217-218:439–444. [PubMed: 22494901]
14. Gupta K, Maity A, Ghosh UC. Manganese Associated Nanoparticles Agglomerate of Iron(III) Oxide: Synthesis, Characterization and Arsenic(III) Sorption Behavior with Mechanis. J. Hazard. Mater. 2010; 184:832–42. [PubMed: 20875700]
15. Shen YF, Tang J, Nie ZH, Wang YD, Ren Y, Zuo L. Tailoring size and structural distortion of Fe_3O_4 nanoparticles for the purification of contaminated water. Bioresour. Technol. 2009; 100:4139–4146. [PubMed: 19414249]
16. Kim J-G, Seo J-W, Cheon J, Kim Y-J. Rietveld Analysis of Nano-crystalline $MnFe_2O_4$ with Electron Powder Diffraction. Bull. Korean Chem. Soc. 2009; 30:183–187.
17. Makris KC, Sarkar D, Parsons JG, Datta R, Gardea-Torresdey JL. X-ray absorption spectroscopy as a tool investigating arsenic(III) and arsenic(V)sorption by an aluminum-based drinking-water treatment residual. J. Hazard. Mater. 2009; 171:980–986. [PubMed: 19631458]
18. Makris KC, Sarkar D, Parsons JG, Datta R, Gardea-Torresdey JL. Surface arsenic speciation of a drinking-water treatment residual using X-ray absorption spectroscopy. J. Colloid Interface Sci. 2007; 311:544–550. [PubMed: 17448489]

19. Makris KC, Sarkar D, Datta R. Evaluating a drinking-water waste by-product as a novel sorbent for Arsenic. Chemosphere. 2006; 64:730–741. [PubMed: 16405955]
20. Genc-Fuhrman H, Tjell JC, McConchie D. Adsorption of Arsenic from Water Using Activated Neutralized Red Mud. Environ. Sci. Technol. 2004; 38:2428–2434. [PubMed: 15116850]
21. Altundogan HS, Altundogan S, Tumen F, Bildik M. Arsenic adsorption from aqueous solutions by activated red mud. Waste Manage. 2002; 22:357–363.
22. Luther S, Borgfeld N, Kim J, Parsons JG. Removal of arsenic from aqueous solution: A study of the effects of pH and interfering ions using iron oxide nanomaterials. Microchem. J. 2012; 101:30–36.
23. Partey F, Norman D, Ndur S, Nartey R. Arsenic sorption onto laterite iron concretions: Temperature effect. J. Colloid Interface Sci. 2008; 321:493–500. [PubMed: 18346752]
24. LeBail A, Duroy H, Fourquet JL. Ab-Initio Structure Determination of $LiSbWO_8$ By X-Ray Powder Diffraction. Mat. Res. Bull. 1988; 23:447–452.
25. Fleet ME. The structure of Magnetite Acta Cryst. 1981; B37:917–920.
26. Kim J-G, Seo J-W, Cheon J, Kim Y-J. Rietveld Analysis of Nano-crystalline $MnFe_2O_4$ with Electron Powder Diffraction. Bull. Korean Chem. Soc. 2009; 30:183–187.
27. Jarosch D. Crystal Structure Refinement and Reflectance Measurements of Hausmannite, Mn_3O_4. Mineral. Petrol. 1987; 37:15–23.
28. Landrot G, Ginder-Vogel M, Livi K, Fitts JP, Sparks DL. Chromium(III) oxidation by three poorly-crystalline manganese(IV) oxides. 1 Chromium(III)-oxidizing capacity. Environ Sci Technol. 2012; 46:1594–600.
29. Zheng Y, Stute M, van Geen A, Gavrieli I, Dhara R, Simpson HJ, Schlosser P, Ahmed KM. Redox control of arsenic mobilization in Bangladesh groundwater. Appl. Geochem. 2004; 19:201–214. THE POINT OF ZERO CHARGE AND ADSORPTION
30. Milonjic SK, Kopecni MM, Ilic ZE. The Point of Zero Charge and Adsorption Properties of Natural Magnetite. J. Radioanal. Chem. 1983; 78:15–24.
31. Backes CA, McLaren RG, Rate AW, Swift RS. Kinetics of Cadmium and Cobalt Desorption from Iron and Manganese Oxides. Soil Sci. Soc. Am. J. 1995; 59:778–785.
32. Jang M, Min SH, Kim TH, Park JK. Removal of arsenite and arsenate using hydrous ferric oxide incorporated into naturally occurring porous diatomite. Environ. Sci. Technol. 2006; 40:1636–1643. [PubMed: 16568781]
33. Guo H, Ren Y, Liu Q, Zhao K, Li Y. Enhancement of Arsenic Adsorption during Mineral Transformation from Siderite to Goethite: Mechanism and Application. Environ. Sci. Technol. 2013; 47:1009–1016. [PubMed: 23252340]
34. Lenoble V, Chabroullet C, al Shukry R, Serpaud B, Deluchat V, Bollinger J-C. Dynamic arsenic removal on a MnO_2-loaded resin. J. Colloid Interface Sci. 2004; 280:62–67. [PubMed: 15476774]
35. Teclu D, Tivchev G, Laing M, Wallis M. Bioremoval of arsenic species from contaminated waters by sulphate-reducing bacteria. Water Res. 2008; 42:4885–4893. [PubMed: 18929386]
36. Deschamps E, Ciminelli VST, Holl WH. Removal of As(III) and As(V) from water using a natural Fe and Mn enriched sample. Water Res. 2005; 39:5212–5220. [PubMed: 16290184]
37. Katsoyiannis IA, Zouboulis AI, Jekel M. Kinetics of bacterial As(III) oxidation and subsequent As(V) removal by sorption onto biogenic manganese oxides during groundwater treatment. Ind. Eng. Chem. Res. 2004; 43:486–493.
38. Gao Y, Mucci A. Individual and competitive adsorption of phosphate and arsenate on goethite in artificial seawater. Chem. Geol. 2003; 199:91–109.
39. Chunming S, Puls RW. Arsenate and arsenite removal by zerovalent iron: effects of phosphate, silicate, carbonate, borate, sulfate, chromate, molybdate, and nitrate, relative to chloride. Environ. Sci. Technol. 2001; 35(22):4562–4568. [PubMed: 11757617]
40. Hongshao Z, Stanforth R. Competitive adsorption of phosphate and arsenate on goethite. Environ. Sci. Technol. 2001; 35(24):4753–4757. [PubMed: 11775149]

Highlights

The binding of As(III) and As(V) to Fe_3O_4, Mn_3O_4 and mixtures of Fe_3O_4-Mn_3O_4 co-synthesized in solution, with approximately 20 nm in diameter was investigated.

The effects of pH and commonly found anions in natural water on the binding of both As(III) and As(V) to the various nanomaterials was studied.

Isotherm studies were performed to determine the capacities of the various nanomaterials.

It was determined that both As(III) and As(V) followed the Langmuir isotherm.

The highest capacity of the nanomaterials was maximized in the 50%Fe-50%Mn with a binding capacity of 41.5 mg/g and 13.9 mg/g for As(III) and As(V), respectively.

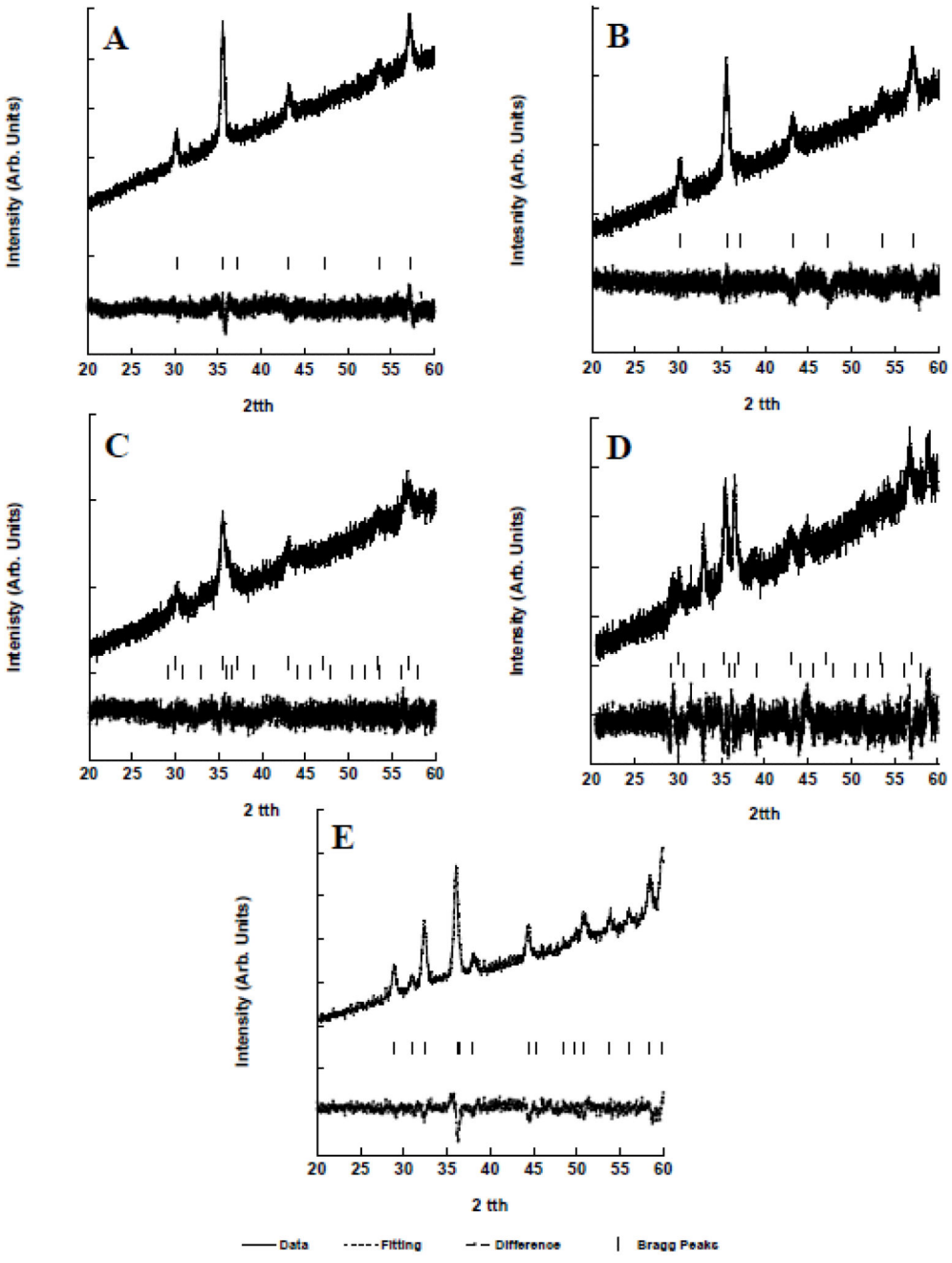

Figure 1.

A. Diffraction pattern for the Fe_3O_4 nanomaterial taken from 20 to 60 in 2θ. **B.** Diffraction pattern for the nanomaterial synthesized from 25%Mn-75% Fe mixture taken from 20 to 60 in 2θ. **C.** Diffraction pattern for the 50% Mn-50% Fe mixture taken from 20 to 60 in 2θ. **D.** Diffraction pattern for the 75% Mn-25% Fe mixture taken from 20 to 60 in 2θ. **E.** Diffraction pattern for the Mn_3O_4 nanomaterial taken from 20 to 60 in 2θ.

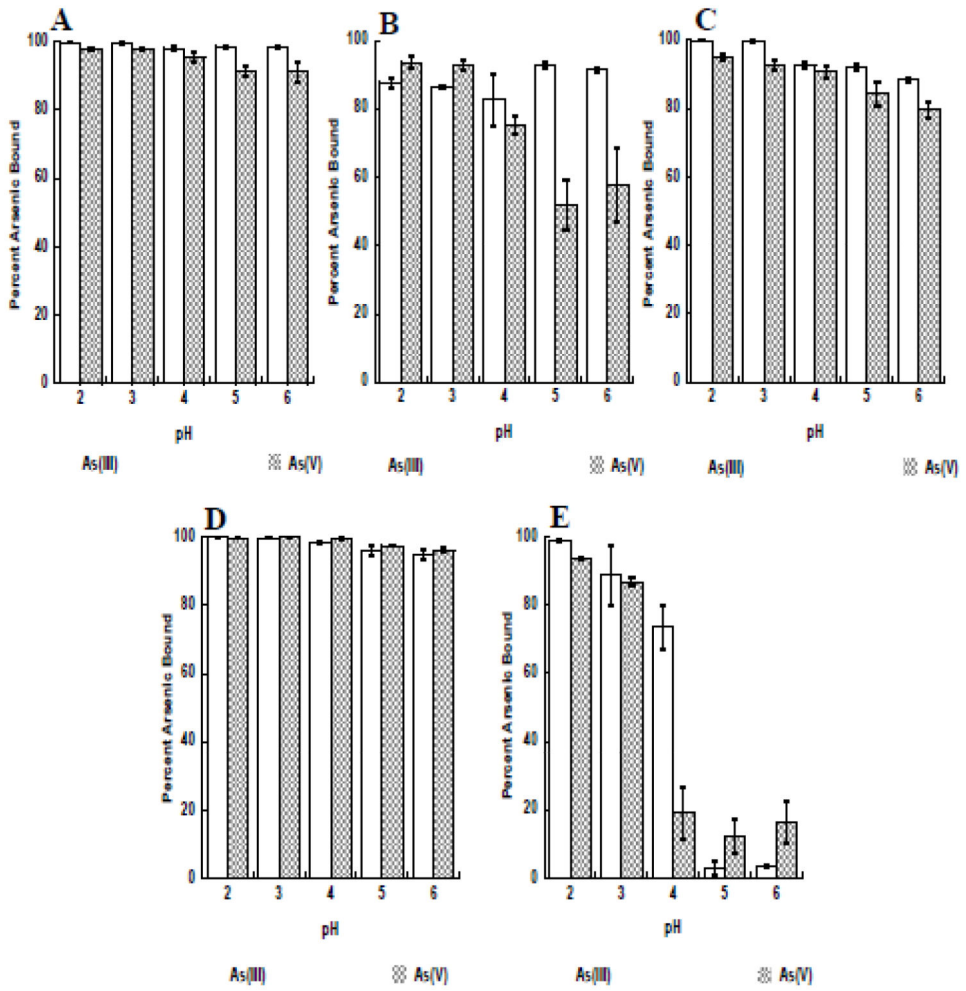

Figure 2.

A. Arsenic(III) and arsenic(V) binding to Fe_3O_4 nanomaterial from pH 2 to pH 6. **B.** Arsenic(III) and arsenic(V) binding to 25% Mn-75%Fe nanomaterial from pH 2 to pH 6. **C**. Arsenic(III) and arsenic(V) binding to 50% Mn-50% nanomaterial from pH 2 to pH 6. **D.** Arsenic(III) and arsenic(V) binding to 75% Mn-25% Fe nanomaterial from pH 2 to pH 6. **E.** Arsenic(III) and arsenic(V) binding to Mn_3O_4 nanomaterial from pH 2 to pH 6.

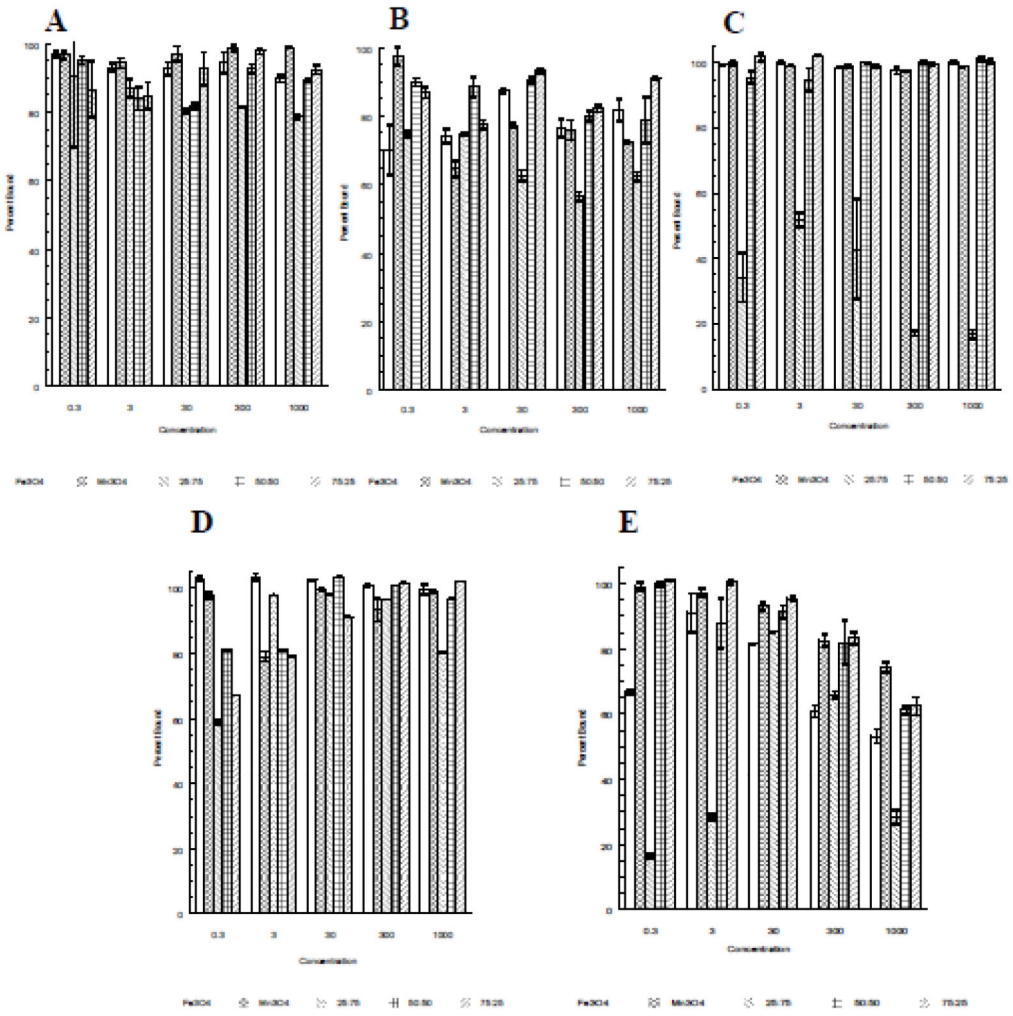

Figure 3.

A. Effect of Cl^{-1} on Arsenic(III) binding to Fe_3O_4, Mn_3O_4, 25% Mn-75%Fe nanomaterial, 50% Mn-50%Fe nanomaterial, and 75% Mn-25%Fe nanomaterial. **B.** Effect of $PO^{3-}{}_4$ on Arsenic(III) binding to Fe_3O_4, Mn_3O_4, 25% Mn-75%Fe nanomaterial, 50% Mn-50%Fe nanomaterial, 75% Mn-25%Fe nanomaterial. **C**. Effect of $NO^{-}{}_3$ on Arsenic(III) binding to Fe_3O_4, Mn_3O_4, 25% Mn-75%Fe nanomaterial, 50% Mn-50%Fe nanomaterial, and 75% Mn-25%Fe nanomaterial. **D.** Effect of $SO^{2-}{}_4$ on Arsenic(III) binding to Fe_3O_4, Mn_3O_4, 25% Mn-75%Fe nanomaterial, 50% Mn-50%Fe nanomaterial, and 75% Mn-25%Fe nanomaterial. **E.** Effect of All interferences on Arsenic(III) binding to Fe_3O_4, Mn_3O_4, 25% Mn-75%Fe nanomaterial, 50% Mn-50%Fe nanomaterial, and 75% Mn-25%Fe nanomaterial..

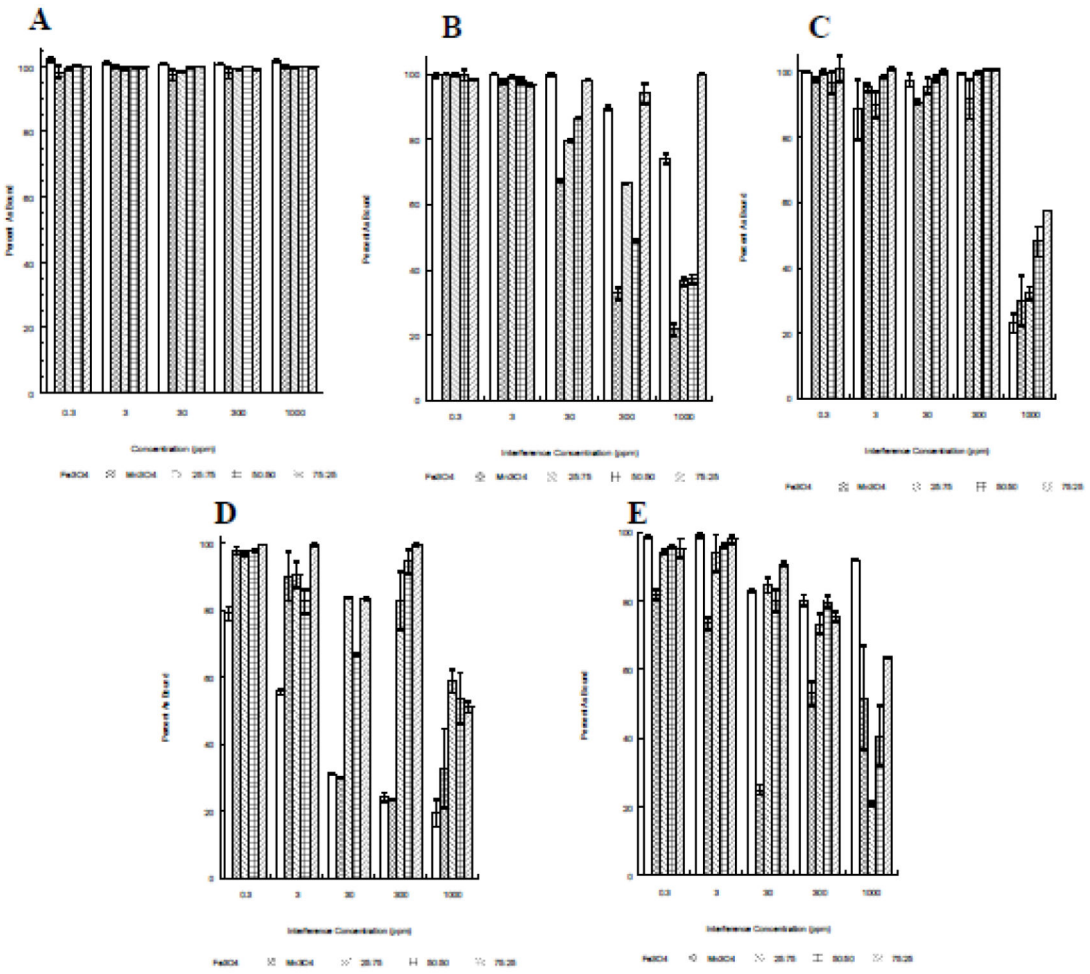

Figure 4.

A. Effect of Cl^{-1} on arsenic(V) binding to Fe_3O_4, Mn_3O_4, 25% Mn-75%Fe nanomaterial, 50% Mn-50%Fe nanomaterial, 75% Mn-25%Fe nanomaterial. **B.** Effect of $PO^{3-}{}_4$ on arsenic(V binding to Fe_3O_4, Mn_3O_4, 25% Mn-75%Fe nanomaterial, 50% Mn-50%Fe nanomaterial, 75% Mn-25%Fe nanomaterial. **C**. Effect of $NO^{1-}{}_3$ on arsenic(V) binding to Fe_3O_4, Mn_3O_4, 25% Mn-75%Fe nanomaterial, 50% Mn-50%Fe nanomaterial, 75% Mn-25%Fe nanomaterial. **D.** Effect of $SO^{2-}{}_4$ on arsenic(V) binding to Fe_3O_4, Mn_3O_4, 25% Mn-75%Fe nanomaterial, 50% Mn-50%Fe nanomaterial, 75% Mn-25%Fe nanomaterial. **E.** Effect of All interferences on arsenic(V) binding to Fe_3O_4, Mn_3O_4, 25% Mn-75%Fe nanomaterial, 50% Mn-50%Fe nanomaterial, 75% Mn-25%Fe nanomaterial.

Table 1

Parameters used for the determination of iron and manganese in the supernatants of the reaction using a Perkin Elmer Optima 8300 DV.

Parameter	Setting
RF Power	1500 W
Nebulizer	Gemcone low flow
Nebulizer Flow	0.65 L/min
Plasma Flow (Ar)	8 L/min
Sample Flow rate	1.25 mL/min
Spray Chamber	Glass Cyclonic
Injector	Alumina 2 mm

Table 2

Crystal lattice parameters for the substitution of Mn^{2+} ions into the Fe_3O_4 lattice and the Mn_3O_4 nanomaterials.

Sample	Cell	a	b	C	α, β, γ
Fe_3O_4	FD-3M	8.396	8.396	8.396	90.0 α= β= γ
$Mn_{0.25}Fe_{2.75}O_4$	FD-3M	8.382	8.382	8.382	90.0 α= β = γ
$Mn_{0.5}Fe_{0.5}O_4$	FD-3M	8.407	8.407	8.407	90.0 α= β= γ
	I41/AMD	5.810	5.810	9.240	90.0 α= β= γ
$Mn_{0.75}Fe_{0.25}O_4$	FD-3M	8.409	8.409	8.409	90.0 α= β= γ
	I41/AMD	5.815	5.815	9.227	90.0 α= β= γ
Mn_3O_4	I41/AMD	5.771	5.771	9.455	90.0 α= β= γ

Table 3

Average grain size determined from the diffraction patterns of the different nanomaterials synthesized.

Sample	Phase	Size (nm)	SE (± nm
Fe_3O_4	Fe_3O_4	19.3	0.8
25% Mn-75%Fe	$Fe_3O_4/Mn_xFe_{3-x}O_4$	17.7	1.1
50% Mn-50%Fe	$Fe_3O_4/Mn_xFe_{3-x}O_4$	19.2	1.3
	Mn_3O_4	ND	ND
75% Mn-25%Fe	$Fe_3O_4/Mn_xFe_{3-x}O_4$	19.3	0.6
	Mn_3O_4	18.7	1.9
Mn_3O_4	Mn_3O_4	15.0	0.5

Table 4

Fitting parameters determined for arsenic(III) and arsenic(V) binding to pure Fe_3O_4, pure Mn_3O_4 and $Mn_xFe_{3-x}O_4$ using Langmuir isotherms.

Material	As(III) $1/Q_0$	R^2	As(V) $1/Q_0$	R^2
Fe_3O_4	0.058	0.999	0.143	1.00
25% Mn-75%Fe	0.060	0.998	0.122	0.99
50% Mn-75%Fe	0.024	1.000	0.073	0.99
75% Mn-25%Fe	0.042	0.998	0.149	1.00
Mn_3O_4	0.065	0.997	0.134	0.99

Table 5

Binding capacities of arsenic(III) and arsenic(V) binding to pure Fe_3O_4, pure Mn_3O_4 and $Mn_xFe_{1-x}O_4$ determined from Langmuir isotherms.

Material	As(III) (mg/g)	SE (± mg/g)	As(V) (mg/g)	SE (± mg/g)
Fe_3O_4	17.1	0.2	7.0	0.2
25% Mn-75%Fe	16.7	0.8	8.2	0.6
50% Mn-75%Fe	41.5	0.4	13.9	0.8
75% Mn-25%Fe	23.8	0.7	7.9	0.4
Mn_3O_4	13.5	0.3	7.5	0.6